

PAPER • OPEN ACCESS

Activation and transmutation of tungsten boride shields in a spherical tokamak

To cite this article: Colin G. Windsor *et al* 2022 *Nucl. Fusion* **62** 036009

View the [article online](#) for updates and enhancements.

You may also like

- [An atom probe tomography and inventory calculation examination of second phase precipitates in neutron irradiated single crystal tungsten](#)
Philip D. Edmondson, Baptiste Gault and Mark R Gilbert
- [Spatial heterogeneity of tungsten transmutation in a fusion device](#)
M.R. Gilbert, J.-Ch. Sublet and S.L. Dudarev
- [Experimental validation of inventory simulations on molybdenum and its isotopes for fusion applications](#)
M.R. Gilbert, L.W. Packer and T. Stainer

Activation and transmutation of tungsten boride shields in a spherical tokamak

Colin G. Windsor^{1,*}, Jack O. Astbury¹, J. Guy Morgan²,
Christopher L. Wilson¹ and Samuel A. Humphry-Baker³

¹ Tokamak Energy Ltd, 173 Brook Drive, Milton Park, Oxon OX14 4SD, United Kingdom

² Culham Electromagnetics Ltd, D5, Culham Science Centre, Abingdon OX14 3DB

³ Dept. of Materials, Imperial College, London SW7 2AZ, United Kingdom

E-mail: colin.windsor@tokamakenergy.co.uk

Received 22 September 2021, revised 13 December 2021

Accepted for publication 5 January 2022


Published 24 January 2022



Abstract

The FISPACT-II code is used to compute the levels of activation and transmutation of tungsten borides for shielding the central high temperature superconductor core of a spherical tokamak fusion power plant during operations at 200 MW fusion power for 30 years and after shutting down for 10 years. The materials considered were W_2B , WB , W_2B_5 and WB_4 along with a sintered borocarbide $B_{0.329}C_{0.074}Cr_{0.024}Fe_{0.274}W_{0.299}$, monolithic W and WC . Calculations were made within shields composed of each material, for five reactor major radii from 1400 to 2200 mm, and for six ^{10}B isotope concentrations and at five positions across the shield. The isotopic production and decay in each shield is detailed. The activation of boride materials is lower than for either W or WC and is lowest of all for W_2B_5 . While isotopes from tungsten largely decay within 3 years of shut-down, those from boron have a much longer decay life. An acceptable 70% of the absorbing ^{10}B isotope will remain after 30 years of operations behind the first wall for a 1400 mm radius tokamak. Gaseous production is problematic in boride shields, where 4He in particular is produced in quantities 3 orders of magnitude higher than in W or WC shields. The FISPACT-II displacements per atom (dpa) tend to increase with boron content, although they decrease with increased ^{10}B isotopic content. The dpa ranges of boride shields tend to lie between those of W and WC . Overall, the results confirm that the favourable fusion reaction shielding properties of W_2B_5 are not seriously challenged by its irradiation and transmutation properties, although helium gas production could be a challenge to its thermal and mechanical properties.

Keywords: spherical tokamaks, tungsten borides, shielding, fispact-II, activation, neutrons, gamma rays

 Supplementary material for this article is available [online](#)

(Some figures may appear in colour only in the online journal)

* Author to whom any correspondence should be addressed.



Original content from this work may be used under the terms of the [Creative Commons Attribution 4.0 licence](#). Any further distribution of this work must maintain attribution to the author(s) and the title of the work, journal citation and DOI.

1. Introduction

The shielding of the high temperature superconductor (HTS) core remains a key component in any possible spherical tokamak fusion power plant. An optimal shielding material needs to reduce the incoming heat load to the HTS core, and to reduce its neutron and gamma radiation damage. It must also be itself resistant to radiation damage, be able to withstand high temperatures, retain adequate isotopic content and remain stable over many years of operation. It must be capable of manufacture in the tonnage quantities necessary for a fusion power plant. In an earlier paper [1] candidate shielding materials containing tungsten and boron were evaluated using the Monte Carlo modelling code MCNP [2]. It confirmed that the inclusion of boron within a tungsten-based shield is advantageous, because of its high neutron absorption cross section at lower energies. It found W_2B_5 to be particularly effective, with its favourable structure, density, and high atomic number densities. Hydride shields have been shown to be highly effective. ZrH_2 and the borohydride $Zr(BH_4)_4$ gave neutron half-attenuation distances of order 50 mm [3] comparable with those reported for tungsten borides [1], although greater than the 40 mm reported for W_2B_5 . Gamma shielding of the heavy metal hydrides BaH_2 and ZrH_2 have been examined [4]. Their gamma half-attenuation distances suggested them as highly effective gamma shielding materials.

Activation and transmutation product formation under fusion neutron irradiation has been reported for several candidate fusion engineering materials [5], particularly in the case of W and W alloys [6]. The activation behaviour of tungsten under neutron irradiation is complex. H and He production is relatively minor, however significant quantities of Re, Ta, and Os will be produced. These elements cause Re and Os-rich clusters and precipitates, leading to material embrittlement [7].

Quantitative assessment of activation product data for the tungsten carbides and borides is yet to be reported. Oliver *et al* [8] proposed that in WC, Re, Ta, and Os production would likely lead to the precipitation of secondary carbides, particularly TaC. Neutron irradiation studies of slightly porous coarse-grained W_2B_5 have led to swelling, embrittlement, and eventual fracture due to helium production [9]. Although the material performed well compared to the other candidate borides based on metals in groups IV–VI (Ti, Zr, Hf, V, Nb, Cr and Mo). Activation product release of He and Li and ^{10}B burn-up have been characterised in neutron irradiated group IV–V metal borides [10], although this study excluded any tungsten borides. Isotopic tailoring of ^{11}B may be necessary if borides are to be used as structural materials [11]. The activation of the core materials including the HTS tapes, their insulation, copper matrix and inconel structure will be discussed in a later paper.

In this study the code FISPACT-II v4.0 [12, 13] is used to study the activation, decay cooling, gas production, and displacements per atom (dpa) of these materials over 30 years operations at 200 MW fusion power, followed by a 10 years cooling-off period. Section 2 describes details of the FISPACT-II calculations used. Section 3 details the shield material activation during operations and radioactive decay during a

10 years cooling-off period. The gamma-ray energy spectrum from the irradiated materials is discussed in section 4. Gaseous transmutation products are concerning because of possible swelling and bubble formation and are considered in section 5. The ^{10}B isotope is necessarily depleted during neutron absorption through the shield and these effects are detailed in section 6. The results of FISPACT-II estimates of radiation damage in terms of dpa are examined in section 7.

2. Computational details

Monolithic shields were chosen along with shields consisting of six layers with water cooling between each layer. For each material the tokamak major radius was varied in 5 steps from 1400 to 2200 mm. For each boride material, the ^{10}B isotopic concentration was varied in 6 steps from 0% to 100%. Five positions across the shield from the plasma-facing side to the HTS-facing side were considered. This gave a total of $(5 \times 6 + 2) \times 5 \times 2 \times 5 = 1600$ FISPACT-II runs which are summarised in the supplementary material (<https://stacks.iop.org/NF/62/036009/mmedia>). Activation computations were made for a constant plasma fusion power of 200 MW, detailed each year up to 30 years. A period of 10 years after shutdown was considered with FISPACT-II solver outputs at 1 h, 1 day, 1 week, 1 month, 6 months, 1, 2, 3, 4, 5 and 10 years. Fluxes were calculated in cells extending vertically ± 200 mm from the reactor mid-plane, where neutron production is concentrated. From the resulting FISPACT-II outputs the following were extracted:

- The major isotopes causing activation with health and decommissioning consequences
- The gaseous isotopes 1H , 2H , 3H , 3He and 4He which might affect thermal and mechanical properties
- The ^{10}B isotope concentration for examining the operational loss of this neutron absorbing isotope
- FISPACT-II dpa estimates of damage
- The gamma energy spectrum of the activation at 13 energies from 0.01 to 10 MeV.

The presence of water channels made only a minor difference to many properties in many cases. Full data for all 84 configurations and 5 positions within the shield are given in the supplementary material.

3. Activation of the shield material

It is helpful to start with a monolithic tungsten shield in order to separate its activation from those of the borides. Figure 1 shows the rise in activation of monolithic tungsten over the 30 years of operating on a linear time scale, followed by its cooling off for 10 years on a logarithmic scale. Activation is plotted only for isotopes with an activity within 10^{-4} of that of the most active isotope. The decay results are qualitatively consistent with reported activation decay data for all the elements under ITER fusion spectra reported by Gilbert *et al* [14].

After the first year of operation the isotopes of most importance for tungsten are ^{185}W , ^{181}W , ^{187}W , ^{183m}W and ^{185m}W .

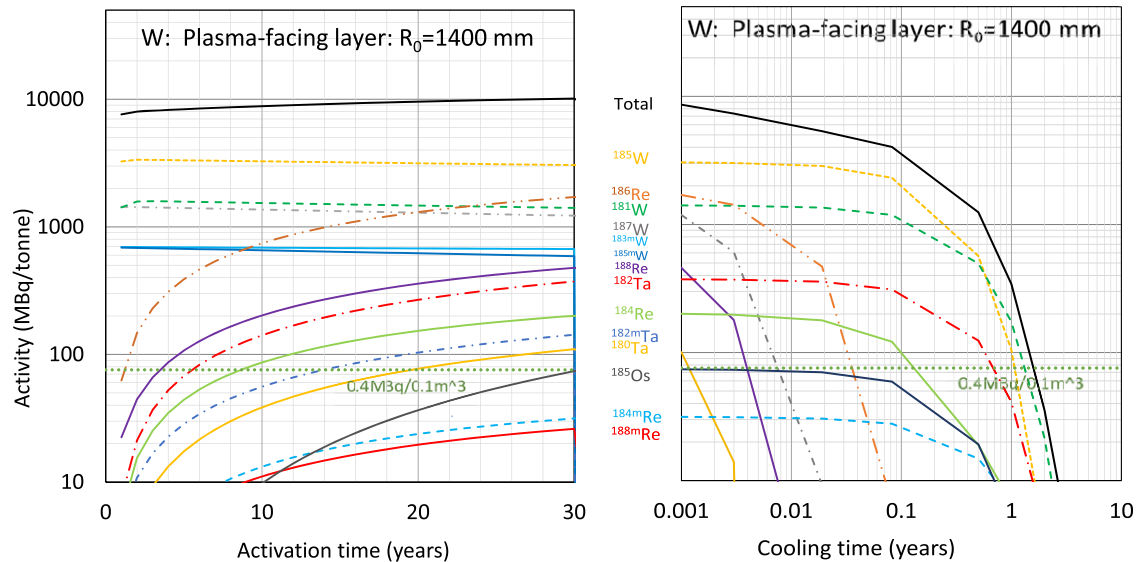


Figure 1. The midplane activation (left) of a monolithic tungsten shield over a 30 years operational period followed by a 10 years cooling-off period (right) for major radius $R_0 = 1400$ mm and for the outer layer of shield where activation will be a maximum. The green dotted horizontal line at $0.4 \text{ MBq}/0.1 \text{ m}^3$ gives an indication of the ‘very low-level waste’ classification [15].

During operations the isotopes ¹⁸⁶Re, ¹⁸⁸Re and ¹⁸²Ta are created by transmutation in significant quantities. ¹⁸⁶Re rises to become the isotope with the second strongest activity. During the 10 years cooling period ¹⁸⁵W and ¹⁸¹W are dominant for the first year while the initially important ¹⁸⁶Re decays within the first month of cooling. After 2 years there is little activity. The limits for disposal as very low-level radioactive waste are dealt with in the Government Department for Environment, Food and Rural Affairs guidance document [15]. Strictly each isotope must be considered individually but for the present purpose the low quantity guidance of 0.4 MBq per 0.1 m^3 ‘dustbin’ volume will be used, as indicated by the leaf-green horizontal dotted lines in figures 1–4.

Figure 2 shows that the boron included in the monolithic W₂B₅ shield gives generally only around half the activation, caused largely by the lower tungsten atomic density in W₂B₅ compared to W. It does introduce ⁸Li as a significant immediate activation product, while tritium ³H is important in the cooling period, where it becomes dominant after about a year. It is noticeable that the actual activation for the W₂B₅ after 30 years of operations is $4005 \text{ MBq}/\text{tonne}$, which is appreciably less than the $10\,120 \text{ MBq}/\text{tonne}$ for monolithic tungsten, despite it being a much better shield. This could be a considerable advantage in the case of a loss-of-coolant event.

Figure 3 compares the activation of all candidate materials after 30 years of operation. The borocarbide B_{0.329}C_{0.074}Cr_{0.024}Fe_{0.274}W_{0.299} shield contains a considerable fraction of iron and chromium and soon builds up ⁵⁵Fe and ⁵⁴Mn isotopes which give the material higher activation at 1400 mm radius than all the other materials considered. Since tungsten itself activates strongly, it is not surprising that the activation generally decreases with boron atomic fraction, but the decrease is not large at the plasma-facing side, because the neutron fluences there are similar. However further into

the shield at lower (and more varied) fluences, the activation depends more strongly on the boron content. The fluence was shown in figure 6 of [1] to depend on boron atomic fraction very much like the activation dependence seen here.

The dashed lines in figure 3 refer to shields containing layers of water for moderation and for cooling, as illustrated in figure 3 of [1]. It is seen that the differences are rather marginal in this case as might be expected from the minor changes in neutron fluence across the shield illustrated in figure 13 of [1]. For the remainder of this paper the effects of water channels will be mentioned only when the differences are noteworthy.

Of importance for decommissioning costs is the activation remaining after a cooling-off period of for example 1 year as shown in figure 4. Except for being an order of magnitude lower, the 1 year cooling activation is remarkably similar to the 30 years operations activation of figure 3, depending mainly on the medium lifetime tungsten isotopes. The dependence on boron fraction is much weaker as the activation is dominated by tungsten. After cooling for periods greater than 5 years the situation is different. The tungsten activity is very much reduced, and as shown in figure 2 for W₂B₅, the boron fraction introduces ³H as an additional longer-lived isotope and the activity after 5 years is only modestly reduced further.

In figure 4 the activation is plotted as a function of distance into the shield. For the boride materials the decay is close to exponential except near the HTS-facing surface. For W and WC shields there is more curvature in these plots. Exponential fits to this region are shown dashed with the half attenuation distances listed for each material in the legend.

While the activation on the plasma-facing surface is similar for all materials with the exception of the borocarbide, the rate of attenuation through the shield varies considerably. W₂B₅ gives the best attenuation with a half-distance attenuation of 36 mm. The other materials have the attenuation half-distances shown in the caption of figure 4.

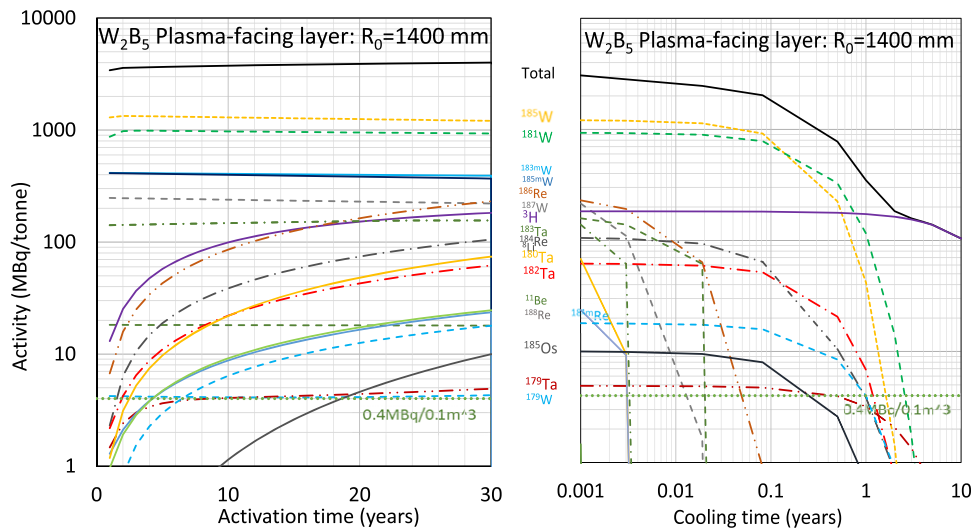


Figure 2. The activation per tonne of W_2B_5 over 30 years operations and cooling times up to 10 years from a monolithic W_2B_5 shield. Note the dominant activity of 3H (tritium: violet colour) in the later stages of cooling. The leaf-green dotted line again represents very low-level waste.

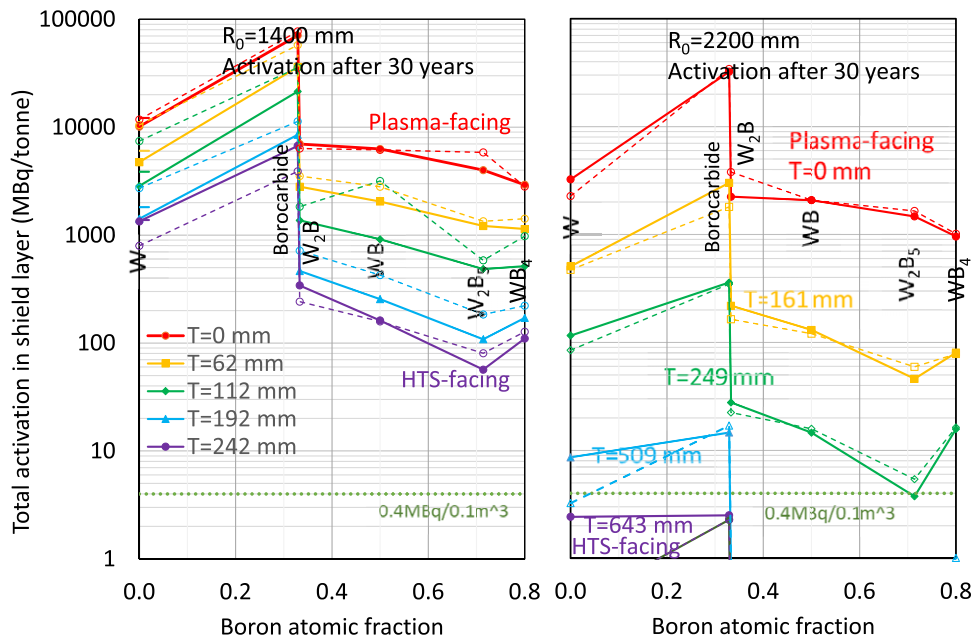


Figure 3. The total midplane activation at various thicknesses T into the shield as a function of the boron atomic fraction of monolithic shields after 30 years of operation. The coloured indents represent the activation for WC shields. Dashed lines and open symbols refer to shields with layers of water. The dotted line again represents very low-level waste.

4. The gamma energy spectrum from the irradiation products

FISPACT-II calculates the energy spectrum of the gamma rays created per unit volume and unit time from the irradiation products. In the present computations the spectrum covered energies between 0.01 and 10 MeV. Figure 5 (left) shows the gamma energy spectrum from activated isotopes for the different materials considered after irradiation for 30 years. The dependence on material can be seen most notably by the marked increase in the spectrum above 2.5 MeV for boride

materials, which increases steadily with boron content. In contrast the spectrum in the range 0.05–1 MeV decreases slightly with boron content, suggesting that emission processes in this range are dominated by tungsten. The spectrum from all the shield materials differs little during the 30 years of irradiation and is therefore not shown.

The centre section of figure 5 shows for a W_2B_5 shield the marked decrease of around two orders of magnitude in activation with distance T into the shield from the plasma-facing to the HTS-facing side. The right section shows the decrease during the 10 years cooling-off period after the 30 years

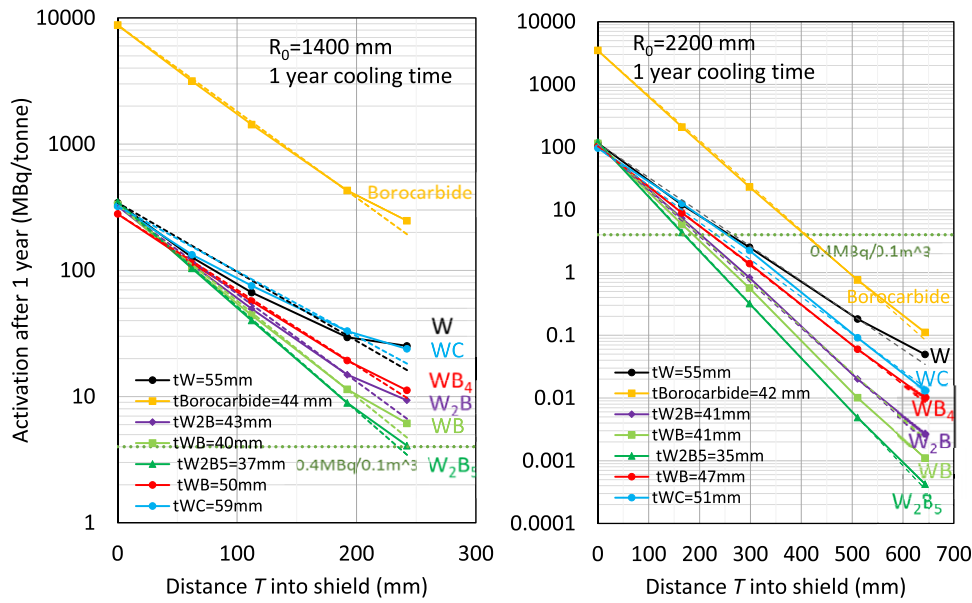


Figure 4. The total activation at various thicknesses T into the shield after 1 year cooling off period following 30 years operation for a major radius of 1400 mm (left) and 2200 mm (right). Dashed lines show an exponential fit to the activation decay with the half distance attenuations t shown in the captions. The green dotted line represents very low-level waste.

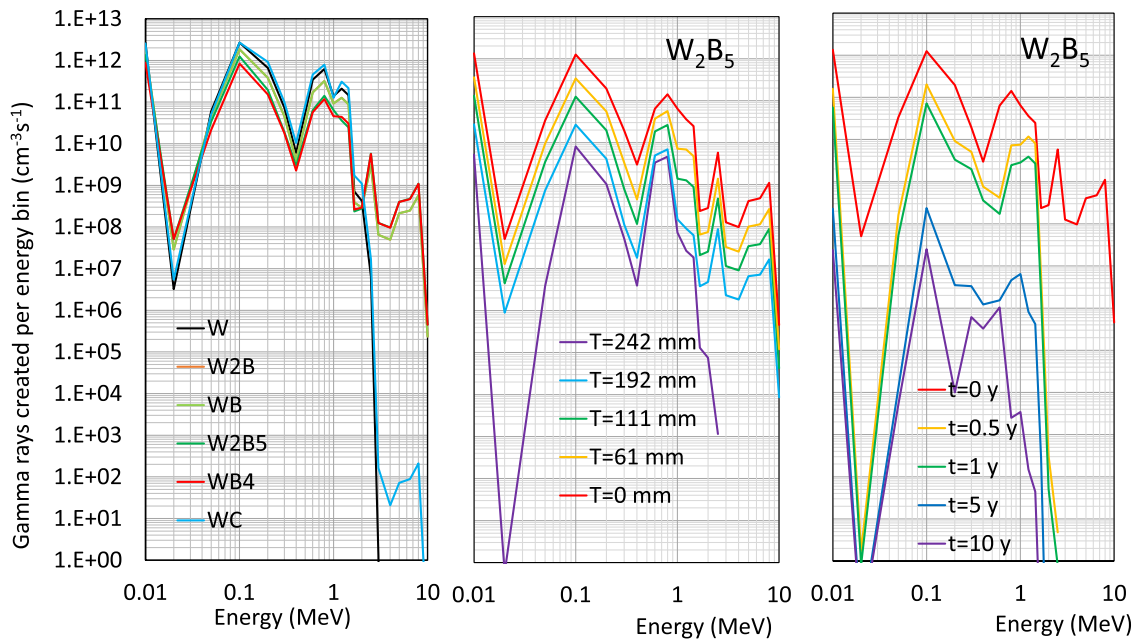


Figure 5. The number of gamma rays created per energy bin, per unit volume, per unit time from irradiated shield materials on the plasma-facing side after irradiation for 30 years in a tokamak of major radius 1400 mm (left). In the centre for a W_2B_5 shield the decrease in irradiation with depth T into the shield is shown. On the right the decrease is shown as a function of the cooling time t in years.

irradiation. There is a drop in activation of at least four orders of magnitude by 10 years, depending on the gamma ray energy. In the first half year there is a drop of around 10 over energies 0.1–2 MeV, but the boron-related activity in the energy range from 2 to 10 MeV drops largely away in this time.

5. The production of gaseous irradiation products

The mechanical and thermal properties of any shield material are likely to be adversely affected by any insoluble gaseous products, which might diffuse to form gas bubbles. This can occur whether the gaseous isotopes produced by irradiation

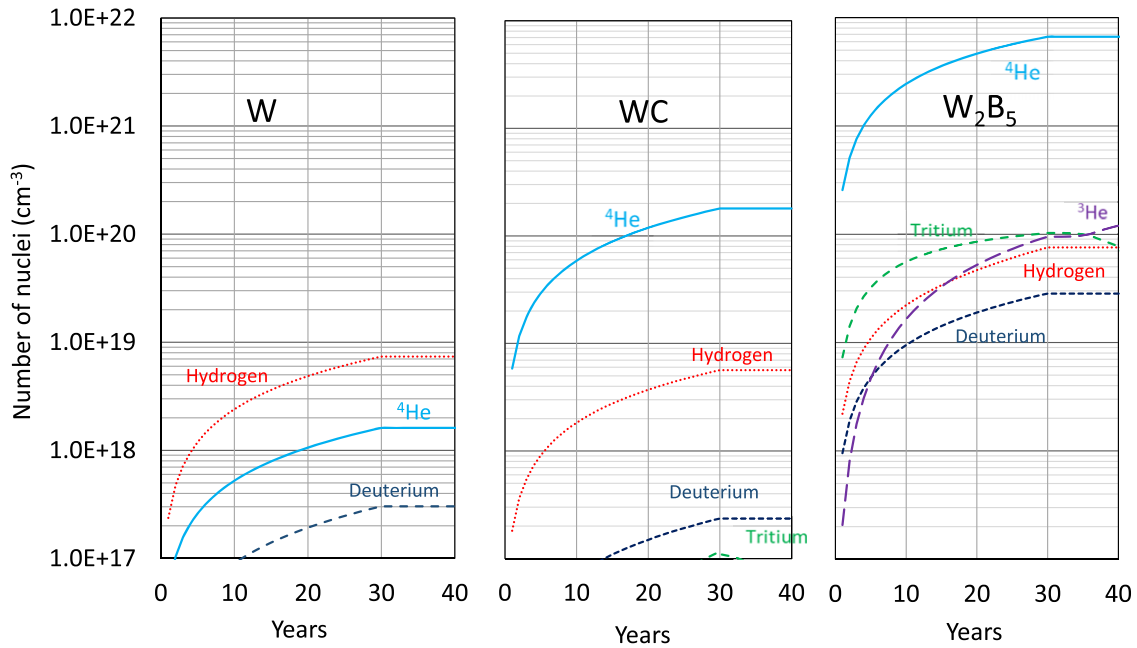


Figure 6. The number of gaseous nuclei produced over an irradiation time of 30 years and a cooling time of 10 years. The results are for the plasma-facing shield layer for a major radius of 1400 mm.

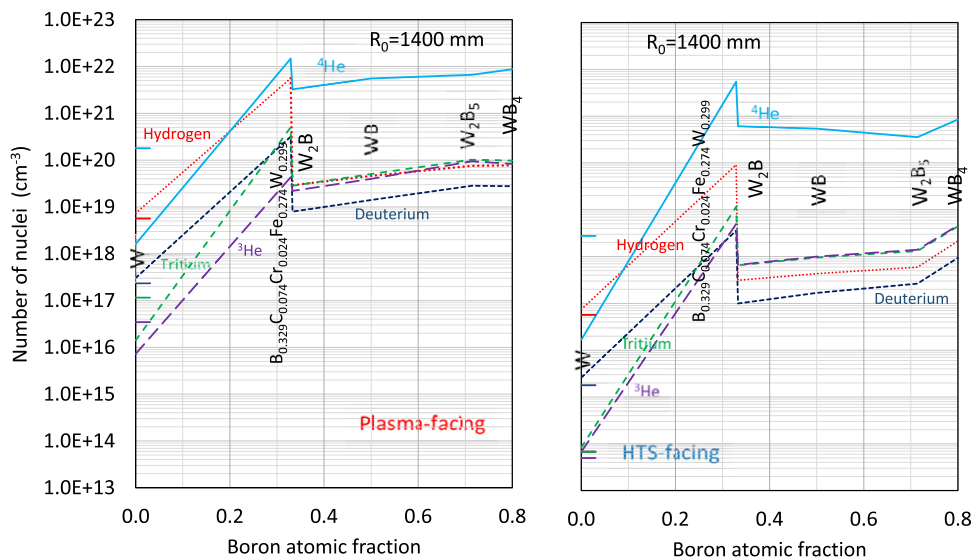


Figure 7. The number of gaseous nuclei produced at an irradiation time of 30 years for the various shield materials for the plasma-facing (left) and HTS-facing sides (right). The WC values are indicated by the coloured indents. The figures have identical scales.

are active or not. The FISPACT-II code was used to identify any such isotopes. For all the shield materials considered, the gaseous isotopes detected in significant quantities included: ordinary hydrogen ^1H , deuterium ^2H , tritium ^3H , helium-3 ^3He , and the alpha particle helium-4 ^4He .

Figure 6 illustrates the production of gaseous nuclei for monolithic W, WC and W_2B_5 , and their decay during the 10 years cool-down. It is seen that with monolithic tungsten the only significant gaseous isotopes are the stable hydrogen, ^4He and deuterium. For WC there is appreciable production of alpha particles ^4He , while the production of hydrogen ^1H and deuterium ^2H is similar.

When boron is present, as with W_2B_5 , the production of gaseous ^4He is increased by another order of magnitude, and the production of ^1H and ^2H is considerably larger, along with the introduction of ^3H and ^3He in appreciable quantities. Looking at years 30 to 40, during the 10 years cooling-off period, there is no change in the stable gaseous isotopes, apart from the decay of tritium producing a small increase in ^3He .

The production of gaseous nuclei as a function of material boron content is summarised in figure 7 for the plasma-facing shields (left) and for the inner HTS-facing shields (right). Note that the two figures are on the same scale. For tungsten shields

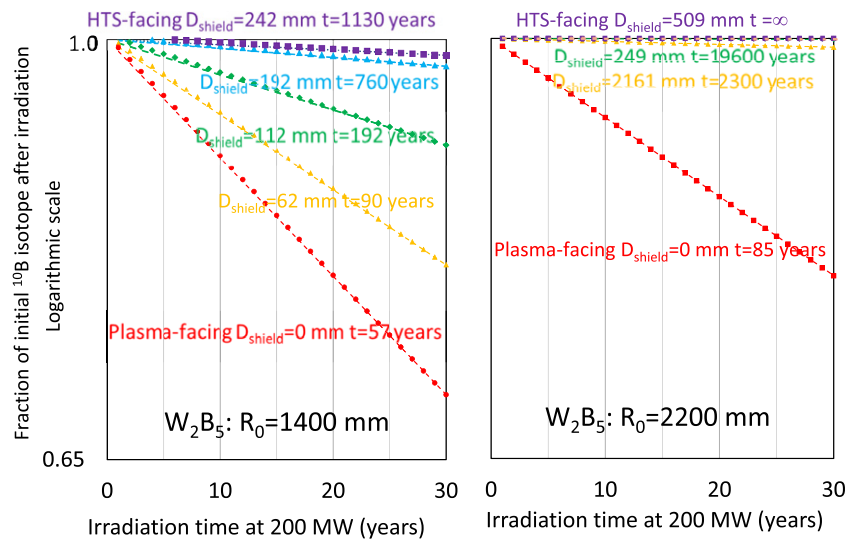


Figure 8. The retained fraction of ^{10}B nuclei within a W_2B_5 shield as a function of irradiation time for different layers within the shield. The data are plotted on a logarithmic scale and the dashed lines correspond to exponential decay with the half time t in years shown in the legend.

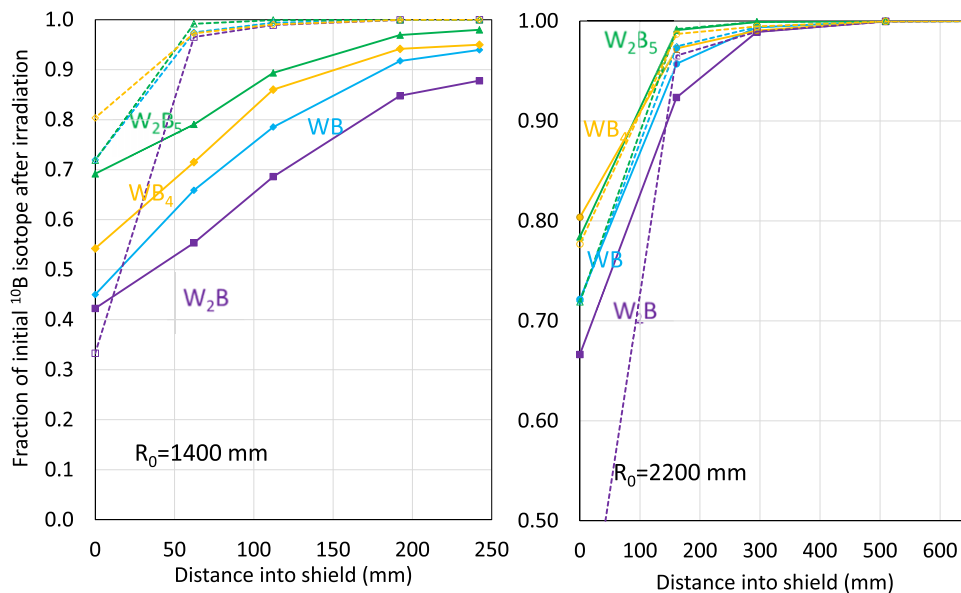


Figure 9. The retention fraction of ^{10}B nuclei after 30 years irradiation within natural tungsten boride shields as a function of distance into the shield for major radii of 1400 mm (left) and 2200 mm (right). The dashed lines are for materials with water channels.

the production of gaseous nuclei is around a factor 100 lower on the HTS-facing side than on the plasma-facing side. Regarding the boride shields, the reduction factor is around 10. For the boride shields, the gaseous production is seen to be dominated by ^4He with the production of other particles being around two orders of magnitude lower. The plasma-facing production of ^4He , ^1H , ^2H , ^3H and ^3He are all seen to increase slightly with boron content, while the HTS-facing production of ^4He decreases up to W_2B_5 where it forms a local minimum, presumably due to W_2B_5 's superior shielding efficiency. Overall, the gaseous production rate throughout all the boride shields is significantly greater than for tungsten. In this case W_2B_5 has no substantial advantage over other borides.

6. The depletion of the ^{10}B isotope during fusion operations

In the boron-containing shield materials considered in this study, the desirable neutron capture by the ^{10}B isotope means that the amount of ^{10}B within the shield material gradually diminishes during operations. The degree of retention has been evaluated using the FISPACT-II code for all relevant materials as a function of time at 5 positions within the shield. Figure 8 illustrates the retention in the concentration of ^{10}B isotope within a W_2B_5 shield at the 5 positions within the shield on a logarithmic plot. The constant slope shows that the retention is close to exponential with the half-intensity decrease time shown inset.

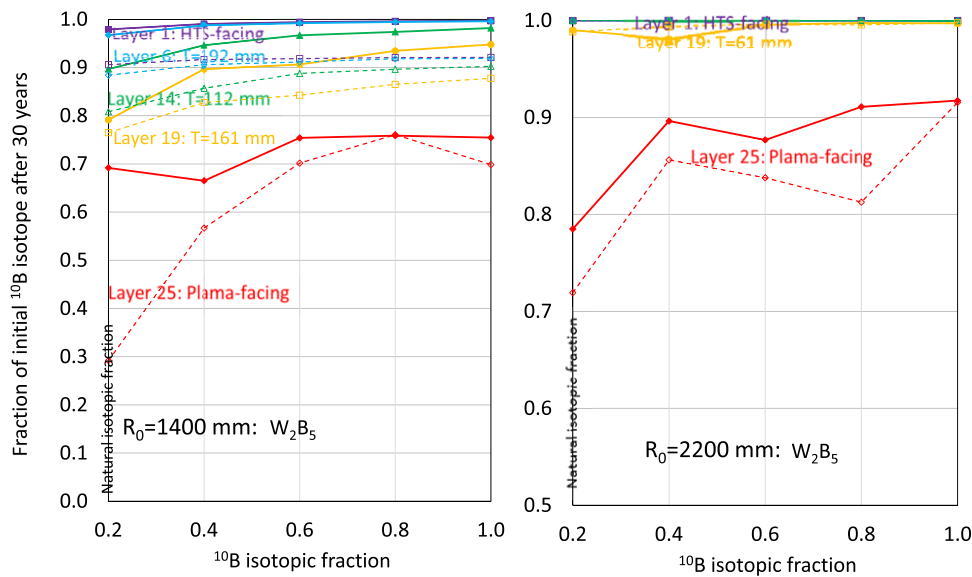


Figure 10. The retention fraction of ^{10}B nuclei over 30 years against the manufactured ^{10}B isotopic fraction for several layers within a W_2B_5 shield of major radii 1400 mm (left) and 2200 mm (right). The dashed lines and open symbols indicate shields with water layers.

It follows that the ^{10}B retention may be well characterized by the 30 years retention fraction. In figure 9 this fraction is plotted as a function of distance into the shield for all the boride shield materials. The results for $R_0 = 1400$ mm (left of figure 9) on the plasma-facing side show the W_2B_5 shield to have an acceptable 70% of the isotope retained after 30 years, with other materials appreciably worse. The retention fraction increases into the shield so that it is over 88% for all materials at the HTS-facing side.

The results for $R_0 = 2200$ mm (right of figure 9) show slightly greater ^{10}B retention on the plasma-facing side. The big difference is that the retention fraction of this isotope increases with depth into the shield at a similar rate, so that it becomes almost totally retained for all materials just half-way into the thicker shield. For thick shields, the results suggest that only the first few layers undergo significant operational depletion, particularly for W_2B_5 . This may mean that only these most exposed layers require replacement or reconfiguration through life. Note that the retention fraction is generally more favourable for the W_2B_5 shield than for all other materials considered in this study.

The dashed lines in figure 9 show the corresponding values for shields containing 5 layers of water occupying roughly 1/5 of the shield total thickness as detailed in [1]. These have a role in cooling the shield but also in moderating the neutrons. The figure shows that including the water layers has an appreciable effect on the ^{10}B retention factor. At a 2200 mm major radius, the plasma-facing fraction tends to decrease, considerably so for W_2B_5 , but then improves more rapidly with distance into the shield soon becoming better than that for monolithic shields. This effect is of practical importance in reducing the operational time before replacement of the plasma-facing layer of the shield due to an unacceptable reduction in the ^{10}B retention fraction.

An increased isotopic concentration of ^{10}B has long been used within the nuclear industry to improve the performance

of neutron absorbing control rods and neutron counters [16]. Because of the 10% difference in nuclear mass between the two isotopes, and the relatively large (20%) natural abundance of the ^{10}B isotope, the concentration can be increased relatively easily for example by gas diffusion [17]. It is available commercially [18]. The improved retention of the ^{10}B isotope over 30 years of operations is shown in figure 10 for W_2B_5 shields with major radii of 1400 and 2200 mm. There is some statistical uncertainty, particularly in the plasma-facing layer, but at all depths in the shield and at both radii, there is a general improvement in isotope retention with ^{10}B concentration. The majority of the possible improvement is achieved by 40% isotopic concentration. It is judged that, because of the rapid increase in retention fraction through the shield, its neutronic performance is unlikely to be appreciably changed. The effects of water-cooling layers in the retention factor are shown by the dashed lines and open symbols. Its effect is again seen to decrease the retention factor.

7. FISPACT-II estimates of radiation displacement damage to the shield

It has been long known that the fast neutron fluences from fusion give rise to extreme levels of radiation damage in materials. Plasma facing materials in a fusion power plant can experience around 100 displacements per atom (dpa) during the lifetime [19]. These lead to formation of point defects and dislocation loops, eventually clustering into voids, which degrade the material properties. Since fusion energies are much higher than atomic displacement energies $E_d \sim 25$ eV the resulting cascade of damage centres can extend over multiple sites. These are best studied by molecular dynamics computations where assumed inter-atomic potentials are used to investigate the nature of the cascades [20]. In the absence of these detailed computations, FISPACT-II has been used to provide a 'useful integral quantity that allows approximate

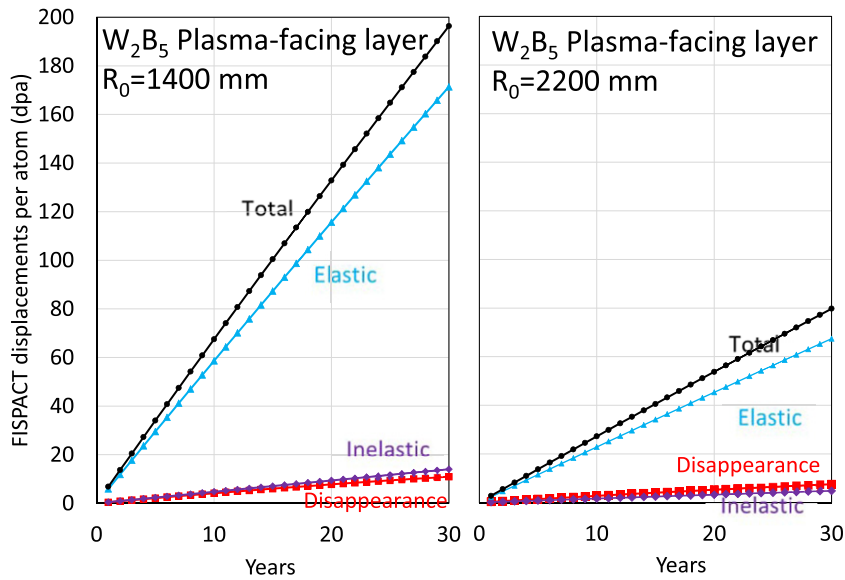


Figure 11. The cumulative dpa values for the outer plasma-facing W_2B_5 shield at major radii 1400 mm (left) and 2200 mm (right). The curves show inelastic, disappearance, elastic and total dpa values.

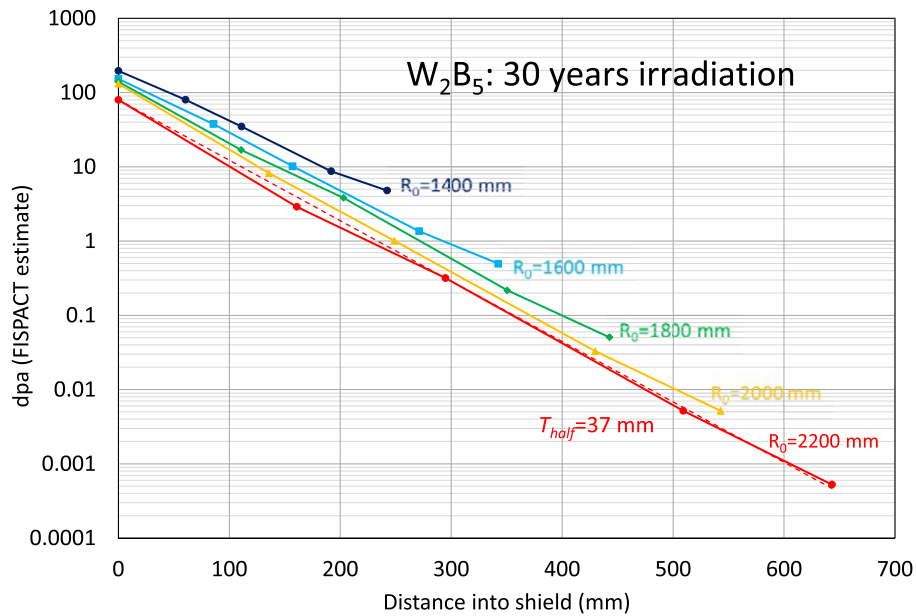


Figure 12. The total cumulative dpa for a monolithic W_2B_5 shield after 30 years of irradiation shown as a function of distance into the shield for all the tokamak major radii. The slope, shown by the dashed line fitted to the 2200 mm radius case, corresponds to a half attenuation thickness T_{half} of 37 mm.

assessment of the respective damage doses experienced by materials under different neutron fields. This has been shown to correlate well with certain experimental trends’ quoting from [21] where FISPACT-II was used to investigate dpa in the DEMO reactor.

The definition of dpa is given in the page 125 of the FISPACT-II manual [13] as

$$D_{tot} = e_d \phi \sum_{i=1}^{N_n} N_i \bar{\sigma}_i / 2E_d.$$

Here e_d is the dpa efficiency factor and is set to 80%, ϕ is the neutron fluence as determined by MCNP, N_i is the

number of atoms of type $i = 1, N_n, \bar{\sigma}_i$ is the dpa reaction cross section and E_d is the displacement energy of each atom as given in table 9 on page 126 of [13]. Figure 11 shows for W_2B_5 shields of major radii 1400 mm and 2200 mm, the FISPACT-II cumulative dpa values for the fluxes at the plasma-facing side of the shield. The dpa is divided into the component from elastic scattering processes, from inelastic processes and from capture or disappearance processes when the particle is lost. All the plots are seen to be very close to linear in irradiation time, so that further discussion will be limited to the 30 years dpa values.

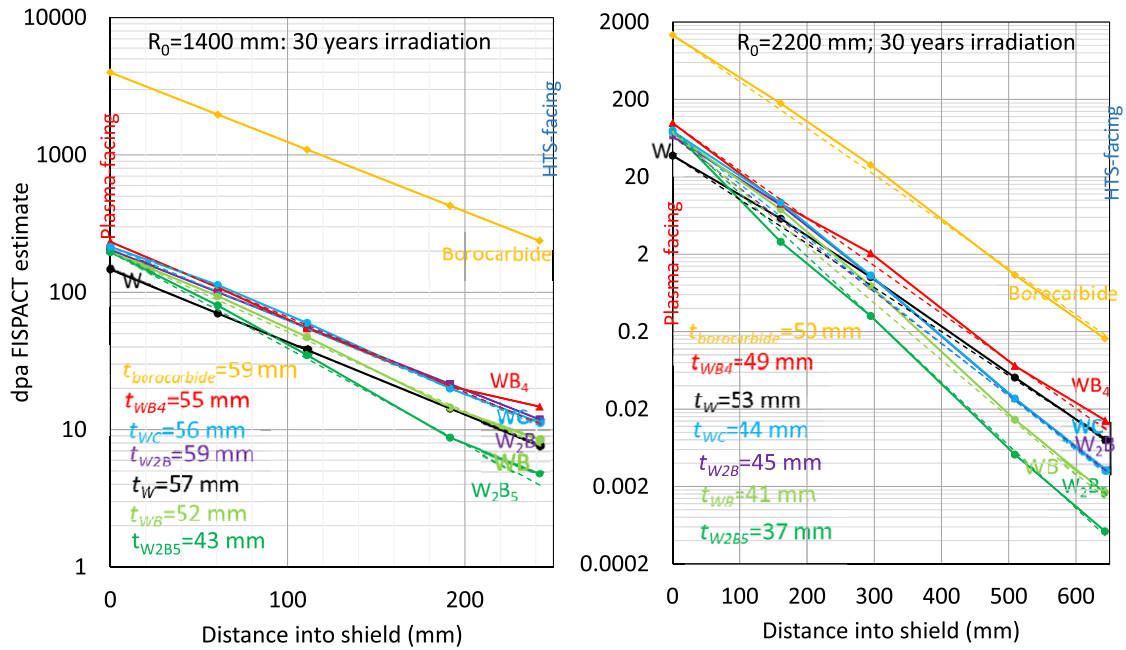


Figure 13. The FISPACT-II estimate of dpa for monolithic shields after 30 years of irradiation shown as a function of distance into the shield. The dashed lines are exponential fits to the data fixed at the plasma facing surface. The half-distance attenuation length is given for each material in the legend.

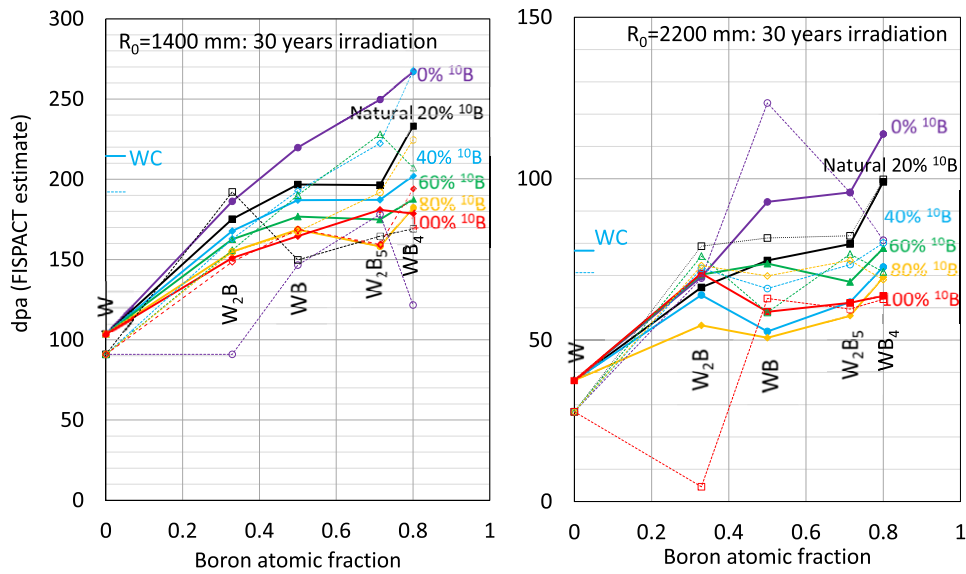


Figure 14. The total cumulative dpa for monolithic shield materials after 30 years of irradiation as a function of the boron atomic fraction for various initial fractions of the ¹⁰B isotopic content. Dotted lines and open symbols are for material shields with water layers. The graphs apply to the plasma-facing side of the shield. The borocarbide has been omitted, being much higher up than the trend. The indented values on the left axis are for WC.

The reduction of the total dpa at 30 years through the layers of the shield for all the major radii is described in figure 12. It is seen that for the 1400 mm device, the dpa values are some 40 times higher on the outer surface than on the inner surface, while for the 2200 mm device, the factor is about 10⁵. The dashed line is a simple exponential of the form $\exp(-\log_e(2)T/T_{\text{half}})$ where T is the distance of the FISPACT-II point into the shield and T_{half} is a half attenuation distance of 37 mm which was close to the attenuation used in figure 7

of [1] for the attenuation of neutron fluence. The dpa reduction half distance is largely independent of major radius.

The dependence of the dpa as a function of distance into the shield for the various shield materials is shown in figure 13. Except for the position nearest to the HTS core, the variation with distance into the shield is close to exponential as shown by the dashed lines. The slope of each line enables an average dpa to be calculated for the complete shield. On the plasma-facing surface the dpa are naturally higher, and there

is an upward trend with boron atomic content. Further into the shield the dpa reduce and the dependence on material boron content becomes more significant and negative, following the neutron flux dependences on boron atomic content shown in figure 7 of [1].

As illustrated in figure 10, there is also the opportunity to use enhanced concentrations of the neutron absorbing isotope ^{10}B . In figure 14 the dpa are shown for all the materials as a function of the ^{10}B isotopic concentration in each boride material. The W and WC values are shown as a reference on the left. The general increase in dpa with boron content noted in figure 11 is matched by a strong ^{10}B isotopic concentration dependence. There is an almost linear increase of dpa with boron content whose slope is greatest at 0% ^{10}B isotopic concentration and decreases with increasing ^{10}B isotopic content. W_2B_5 appears anomalous in that the 100% concentration gives a rather larger dpa than the 80%. The presence of water layers in the shield has only a marginal effect.

8. Conclusions

The activation and damage characteristics of several tungsten boride materials subjected to 30 years of operations at 200 MW followed by 10 years of cooling off have been examined and compared with conventional tungsten and tungsten carbide shields.

The boride shields activate less than pure tungsten or tungsten carbide. In particular W_2B_5 activates least of all the materials considered at positions in the shield away from the plasma-facing surface. This remains true after one year of cooling off, although after 5 years cooling the slow decay of the tritium produced becomes the dominant activation product, so that pure W has lower activity than W_2B_5 after that time.

Gaseous nuclei, particularly ^4He , ^3H (tritium), ^3He , ^2H (deuterium) and ^1H (hydrogen) are produced in appreciably greater quantities by the boride shields, than is the case for W or WC. This could be detrimental for thermal and mechanical properties and in the case of helium could lead to swelling. The general increase with boron content means that W_2B_5 has no advantage in this respect. This highlights the importance of future work to develop strategies to manage the helium inventory and mitigate swelling of the material.

^{10}B has a large absorption cross section which is clearly key to its good neutronics performance in shields. Every neutron absorption produces ^4He and ^7Li so that the fraction of ^{10}B in the shield decreases during operations. The retained fraction is shown to be never less than 70% during 30 years of operations for W_2B_5 . The material performs better in this respect than any of the other borides considered. The rapid increase in retained fraction with distance into the shield from the plasma-facing surface means that the overall depletion of ^{10}B is very small. The presence of water layers in the shield generally decreases the retained fraction of ^{10}B .

Displacements per atom (dpa totals) calculated using the FISPACT-II code were found to be comparable to those for W or WC and decrease rapidly into the shield with at half attenuation distance of order 50 mm. The dpa generally increase with

boron atomic fraction in the plasma-facing side of the shield but decrease with ^{10}B isotopic content. The dpa for W_2B_5 shields are among the lowest of the borides because of the lower neutron fluxes in this material; this suggests that if the expected swelling of W_2B_5 can be mitigated then the longevity of the material with enriched ^{10}B may be increased since the increased neutron capture macroscopic cross-section reduces the neutron flux, which in turn reduces the dpa.

References

- [1] Windsor C.G., Astbury J.O., Davidson J.J., McFadzean C.J.R., Morgan J.G., Wilson C.L. and Humphry-Baker S.A. 2021 Tungsten boride shields in a spherical tokamak fusion power plant *Nucl. Fusion* **61** 086018
- [2] Werner C.J. *et al* 2018 *MCNP Version 6.2 Release Notes Report LA-UR-18-20808* Los Alamos National Laboratory (<https://permalink.lanl.gov/object/tr?what=info:lanl-repo/lareport/LA-UR-18-20808>)
- [3] Hayashi T., Tobita K., Nakamori Y. and Orimo S. 2009 Advanced neutron shielding material using zirconium borohydride and zirconium hydride *J. Nucl. Mater.* **386–388** 119–21
- [4] Vishwanath P.S. and Badiger N.M. 2014 Effective atomic weight, effective atomic numbers and effective electron densities of hydride and borohydride metals for fusion reactor shielding *J. Fusion Energy* **33** 386–92
- [5] Gilbert M.R., Dudarev S.L., Nguyen-Manh D., Zheng S., Packer L.W. and Sublet J.-Ch. 2013 Neutron-induced dpa, transmutations, gas production, and helium embrittlement of fusion materials *J. Nucl. Mater.* **442** S755–60
- [6] Gilbert M.R. and Sublet J.-Ch. 2011 Neutron-induced transmutation effects in W and W-alloys in a fusion environment *Nucl. Fusion* **51** 043005
- [7] Garrison L.M., Katoh Y. and Kumar N.A.P.K. 2019 Mechanical properties of single-crystal tungsten irradiated in a mixed spectrum fission reactor *J. Nucl. Mater.* **518** 208–25
- [8] Oliver S.X., Jackson M.L. and Burr P.A. 2020 Radiation-induced evolution of tungsten carbide in fusion reactors: accommodation of defect clusters and transmutation elements *ACS Appl. Energy Mater.* **3** 868–78
- [9] Grinik E.U., Ogorodnikov V.V. and Krainy A.G. 1996 Fracturing of borides under neutron irradiation *J. Nucl. Mater.* **233–237** 1349–54
- [10] Hoyt E.W. and Zimmerman D.L. 1962 Radiation Effects in borides: I. Helium release and swelling in irradiated borides *Report GEAP-3743 (Pt. 1)* US Atomic Energy Commission (<https://doi.org/10.2172/1098140>)
- [11] Bhattacharya A., Parish C.M., Koyanagi T., Petrie C.M., King D., Hilmas G., Fahrenholtz W.G., Zinkle S.J. and Katoh Y. 2019 Nano-scale microstructure damage by neutron irradiations in a novel boron-11 enriched TiB_2 ultra-high temperature ceramic *Acta Mater.* **165** 26–39
- [12] Sublet J.-Ch., Eastwood J.W., Morgan J.G., Gilbert M.R., Fleming M. and Arter W. 2017 FISPACT-II: an advanced simulation system for activation, transmutation and material modelling *Nucl. Data Sheets* **139** 77–137
- [13] Fleming M., Stainer T. and Gilbert M. (ed) 2018 The FISPACT-II user manual *Report UKAEA-R(18)001* UKAEA (https://fispact.ukaea.uk/_documentation/UKAEA-R18001.pdf)
- [14] Gilbert M.R., Sublet J.-Ch. and Turner A. 2016 Handbook of activation, transmutation, and radiation damage properties of the elements and of ITER materials simulated using FISPACT-II and TENDL-2015; ITER FW armour focus *Report CCFE-R(16)37* (<https://fispact.ukaea.uk/wp-content/uploads/2016/10/CCFE-R1637.pdf>)

- [15] DEFRA 2018 *Scope of Exemptions from the Radioactive Substances Legislation Guidance Document* (https://assets.publishing.service.gov.uk/government/uploads/system/uploads/attachment_data/file/731733/RSL_Guidance_update_BEIS_format_v5_180803.pdf)
- [16] Potapov S.P. 1962 Application of stable boron isotopes *Sov. J. At. Energy* **10** 234–41
- [17] Wang Y.B., Pei G., Jiang D.J. and Zhou M.S. 2020 Economic estimation of boron isotope production by gas diffusion method using BF_3 as processing gas *J. Phys.: Conf. Ser.* **1696** 01200
- [18] American Elements 2021 *Boron-10 Isotope* Los Angeles, CA 90024 USA (<https://americanelements.com/boron-10-isotope-14798-12-0>)
- [19] Humphry-Baker S.A. and Smith G.D.W. 2018 Shielding materials in the compact spherical tokamak *Phil. Trans. R. Soc. A* **377** 20170443
- [20] Nordlund K. *et al* 2018 Primary radiation damage: a review of current understanding and models *J. Nucl. Mater.* **512** 450–79
- [21] Federici G., Biel W., Gilbert M.R., Kemp R., Taylor N. and Wenninger R. 2017 European DEMO design strategy and consequences for materials *Nucl. Fusion* **57** 092002